Winter QPF Sensitivities to Snow Parameterizations and Comparisons to NASA CloudSat Observations

Andrew Molthan[1,2], John M. Haynes[3], Gary J. Jedlovec[2], and William M. Lapenta[4]

[1]*University of Alabama in Huntsville, Huntsville, AL*

[2]*Short-term Prediction Research and Transition (SPoRT) Center, NASA/MSFC, Huntsville, AL*

[3]*Colorado State University, Fort Collins, CO*

[4]*NOAA/NWS/NCEP Environmental Modeling Center, Camp Springs, MD*

1. Introduction

Steady increases in computing power have allowed for numerical weather prediction models to be initialized and run at high spatial resolution, permitting a transition from larger scale parameterizations of the effects of clouds and precipitation to the simulation of specific microphysical processes and hydrometeor size distributions. Although still relatively coarse in comparison to true cloud resolving models, these high resolution forecasts (on the order of 4 km or less) have demonstrated value in the prediction of severe storm mode and evolution (Kain et al. 2008) and are being explored for use in winter weather events (Bernardet et al. 2008). Several single-moment bulk water microphysics schemes are available within the latest release of the Weather Research and Forecast (WRF) model suite, including the NASA Goddard Cumulus Ensemble, which incorporate some assumptions in the size distribution of a small number of hydrometeor classes in order to predict their evolution, advection and precipitation within the forecast domain. Although many of these schemes produce similar forecasts of events on the synoptic scale, there are often significant details regarding precipitation and cloud cover, as well as the distribution of water mass among the constituent hydrometeor classes (Tao et al. submitted).

Unfortunately, validating data for cloud resolving model simulations are sparse. Field campaigns require in-cloud measurements of hydrometeors from aircraft in coordination with extensive and coincident ground based measurements. Radar remote sensing is utilized to detect the spatial coverage and structure of precipitation. Here, two radar systems characterize the structure of winter precipitation for comparison to equivalent features within a forecast model: a 3 GHz, Weather Surveillance Radar-1988 Doppler (WSR-88D) based in Omaha, Nebraska, and the 94 GHz NASA CloudSat Cloud Profiling Radar (Stephens et al. 2002), a spaceborne instrument and member of the afternoon or "A-Train" of polar orbiting satellites tasked with cataloguing global cloud characteristics (Fig. 1). Each system provides a unique perspective. The WSR-88D operates in a surveillance mode, sampling cloud volumes of Rayleigh scatterers where reflectivity is proportional to the sixth moment of the size distribution of equivalent spheres. The CloudSat radar provides enhanced sensitivity to smaller cloud ice crystals aloft, as well as consistent vertical profiles along each orbit. However, CloudSat reflectivity signatures are complicated somewhat by resonant Mie scattering effects and significant attenuation in the presence of cloud or rain water. Here, both radar systems are applied to a case of light to moderate snowfall within the warm frontal zone of a cold season, synoptic scale storm. Radars allow for an evaluation of the accuracy of a single-moment scheme in replicating precipitation structures, based on the bulk statistical properties of precipitation as suggested by reflectivity signatures.

Corresponding author: Andrew L. Molthan. E-mail: andrew.molthan@nasa.gov.

2. Data and Methodology

Throughout the day of February 13, 2007, a mature midlatitude cyclone was traversing the Southern Plains, generating intense convection across Mississippi and Arkansas, as well as extensive snowfall from Nebraska through Ohio. These extensive areas of precipitation are common throughout the cold season months, pose a significant forecast challenge in precipitation quantity and type, and are of widespread economic impact. A portion of this system was sampled by the NASA CloudSat radar during a descending orbit across western Iowa and eastern Nebraska, and was well sampled by the WSR-88D in Omaha (Fig. 1). These radar systems each provide a snapshot of precipitation structures

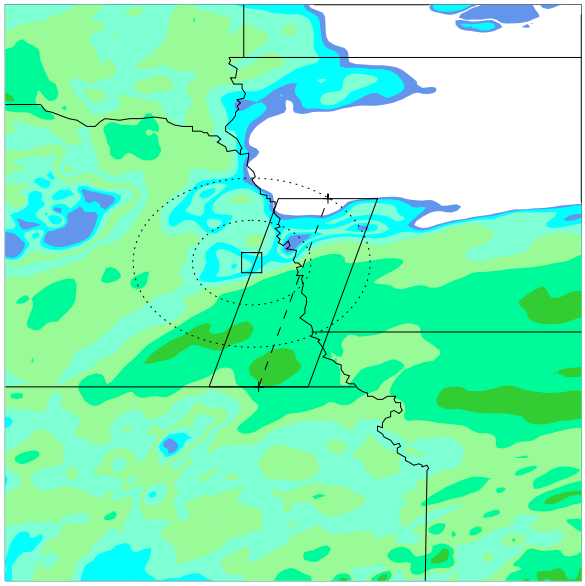

Fig. 1. Domain of interest for the February 13, 2007 case study, depicting the location of the CloudSat flight track (dashed line), subset polygon of WRF model vertical profiles used in radar analyses (parallelogram), the location of the WSR-88D at Omaha, Nebraska (square) and radar range rings at 50 km intervals. Shading depicts lowest model level WSR-88D reflectivity as simulated by the SDSU for conditions in the default Goddard scheme, and focuses on a region northwest of a surface low that was located in central Arkansas. The forecast is valid at 0800 UTC, February 13, 2007.

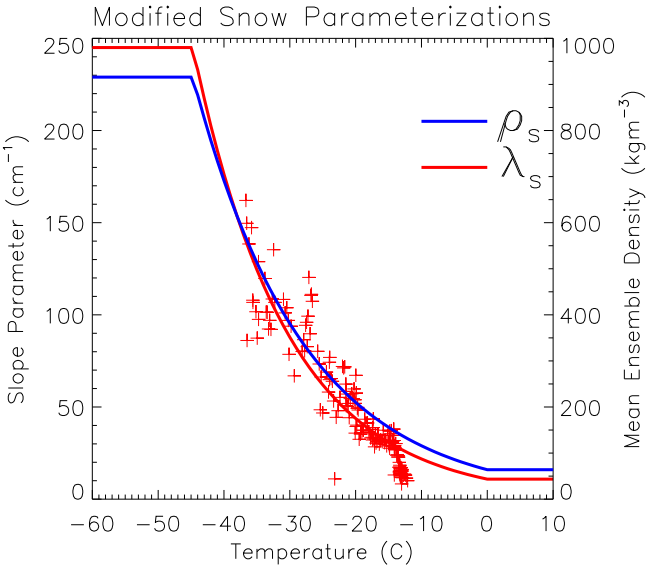

Fig. 2. Snow distribution parameterizations utilized within the experimental forecast based on references in text and C3VP campaign spiral data. Slope parameter values are capped to maintain reasonable values of snow density that are not less than observations, or greater than pure ice. Crosshairs represent observed pairings of air temperature and slope parameter used in the creation of the best fit equation of the form of Ryan (2000).

active within the region and are compared to model equivalents using 3 and 94 GHz radar returns simulated with the Satellite Data Simulator Unit (SDSU hereafter, Matsui et al. 2008). The SDSU provides an estimate of vertical radar reflectivity profiles for terrestrial or spaceborne systems based on the characteristics of the active sensor, hydrometeor quantities and their prescribed size distributions.

Comparisons of simulated clouds to observations require a reasonably accurate forecast that depicts the correct placement of both synoptic and mesoscale features. Given successes in forecasting the evolution of severe weather events, the configuration of the NSSL Spring Experiment (Kain et al. 2008) is replicated here, with the exception being that the NASA Goddard six-class single-moment bulk water microphysics scheme is used as the control experiment. The NASA Goddard scheme (Tao et al. submitted) provides a forecast of six water classes: vapor, cloud water, cloud ice, rain, snow and graupel, where the size distributions of precipitating hydrometeors are fit to an inverse-exponential form, using a fixed intercept and density, with the slope parameter calculated based upon water content.

An experimental forecast is generated that parameterizes the slope parameter of the snow crystal size distribution as a function of temperature, using an equation similar in form to Ryan (2000) but based instead on snow crystal size distributions observed during an aircraft spiral within a similar, synoptic scale snowfall event that occurred during the Canadian CloudSat/CALIPSO Verification Project (C3VP, Hudak et al. (2006)). Heymsfield et al. (2002) advocate for improved snow parameterizations that incorporate a variation in density and Heymsfield et al. (2004) provide an example of snow density parameterizations based upon the distribution slope parameter. Snow density decreases with decreases in slope, suggesting a transition to lower density aggregates. In the experimental forecast, snow density is parameterized with the slope parameter, again based upon C3VP aircraft spiral data. Modifications to the Goddard scheme are summarized in (Fig. 2), otherwise, both forecasts are based upon equivalent initializations and other physical parameterizations.

Although both forecasts provide a reasonable simulation and depiction of observed conditions, some caution must be applied when comparing the characteristics of modeled and observed cloud structures. Model fore-

casts provide results at a particular snapshot in time, which do not coincide with either radar system, even if the forecast is perfect in timing, spatial coverage and intensity. Therefore, verification is performed by examining the characteristics of clouds in a statistical sense, applying contoured frequency with altitude diagrams (CFADs, Yuter and Houze 1995) to forecast model profiles within 0.5 degrees of the CloudSat flight track. The CloudSat radar system provides a much higher spatial resolution (500 m vertical, 1.2 km horizontal) than is available within the forecast model, with a reported minimum detectable reflectivity of -28 *dBZ*. A quality control mask retains radar returns that are most likely cloud, with some signal lost in the lowest 1 km due to surface clutter. In this case, CloudSat sampled light to moderate snowfall at 0840 UTC across eastern Nebraska and western Iowa. All of the CloudSat profiles are retained at full resolution but are combined into a CFAD using the mean altitude ranges of the 34 forecast vertical levels and histogram bin sizes 2 dBZ in order to provide a depiction comparable to the capabilities within the forecast model. In all model forecast analyses, the eighth forecast hour (valid at 0800 UTC on February 13) is used and deemed representative of conditions observed by each radar system.

Verification with the WSR-88D system is complicated by variations in the radar scanning strategies and degradation in minimum detectable signal with range. In order to compensate, modeled reflectivity coverage is reduced to conform to the sampling characteristics of the KOAX radar, based on suggestions by Miller et al. (1998). The KOAX radar was sampling in surveillance mode, volume coverage pattern (VCP) 31, providing only four radar tilts from 0.5 to 4.5 degrees. Volume scans from 0730 to 0830 UTC are used to coincide with the forecast model valid time of 0800 UTC. Model profiles range from approximately 10 to 120 km from the radar location, and in some cases, simulated reflectivity occurs outside the potential scanning range or return capabilities of the WSR-88D. Radar range and model mass level altitude is used to estimate a required KOAX tilt angle, and model points outside of the 0.5 to 4.5 degree tilt range are neglected. In addition, the WSR-88D minimum detectable reflectivity is calculated based upon Miller et al. (1998), and any model reflectivity below the radar detectable signal is removed (Fig. 3). Simulated radar data are reduced in coverage to accomodate the sampling characteristics of KOAX (Fig. 4). Finally, the CFAD technique is applied to the simulated WSR-88D data using histogram bin sizes of 2 dBZ on each model vertical level. Observed

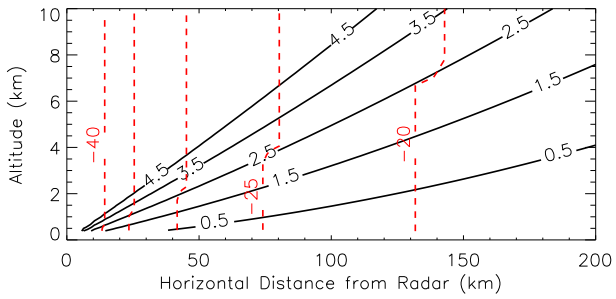

Fig. 3. Minimum detectable radar reflectivity (dBZ, dashed) expected from the WSR-88D in Omaha, Nebraska based on beam tilt angles (degrees, solid) available in surveillance volume coverage pattern 31 and calibration specifications cited by Miller et al. (1998).

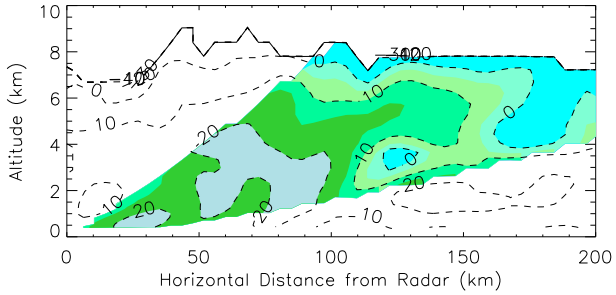

Fig. 4. Demonstration of acceptable WRF simulated reflectivity (dBZ) along a roughly east-west cross section through the WSR-88D location, where color filled reflectivity would be retained in CFAD analyses, in accordance with the actual radar volume sampling coverage.

WSR-88D data are gridded to a Cartesian volume with horizontal and vertical resolution of 1 and 0.5 km, respectively, using a Cressman weighting scheme, and only radar profiles within the 0.5 degree distance from the CloudSat flight track are utilized in comparisons. No additional editing was applied to the WSR-88D reflectivity prior to gridding or CFAD analyses, and only returns greater than -20 *dBZ* are considered.

3. Results and Discussion

Despite significant changes to the formulation of the microphysics scheme, the control and experimental forecasts are similar, at least in a qualitative sense. Both are able to produce broad areas of stratiform precipitation to the northeast of the surface low in advance of the surface warm front, as well as vigorous convection into Arkansas and Mississippi (not shown). In order to examine changes in the three-dimensional structure of simulated clouds, WRF model profiles were extracted within a half degree wide polygon along the CloudSat flight track (Fig. 1). A forecast snapshot, valid at 0800

UTC was chosen to be representative of conditions observed by the CloudSat and WSR-88D systems. The CFAD technique is applied to the hydrometeor contents of these profiles, as well as simulated CloudSat and WSR-88D reflectivity in order to understand potential variability in the microphysical character of simulated precipitation and their remotely sensed characteristics.

a. Hydrometeor Content

Although this simulation is performed with a six-class scheme capable of producing graupel, no significant amounts of graupel were simulated within the subset polygon. Therefore, analyses will focus on the production of snow, cloud ice, and cloud water. The CFAD technique is applied to hydrometeor contents on each of the available model levels, at bin sizes of 0.05 gm^{-3} for precipitating and 0.025 gm^{-3} for nonprecipitating classes. Snow content exhibits a bimodal character below 5 km, likely a result of variable intensity among precipitation within the frontal zone. Similar variability was noted in the radar reflectivity from KOAX during the period. Cloud water content displays a single mode with two peaked levels near 2 and 4 km, while cloud ice is concentrated above 5 km, then scoured out as snow crystals continue to form through accretion processes. By comparison, the experimental forecast suggests a minor increase in snow content, in both the modal value and extremes at the tails of the probability distributions. The maximum values of cloud water are also increased at levels where peaks were already present. Finally, although there is not much change above 5 km, cloud ice is slightly increased below this level.

Although it is difficult to determine the precise cause of these changes, idealized calculations were performed for selected microphysical source and sink terms (Fig. 6). These estimations assume the case of sea level pressure (1013.25 hPa), saturation with respect to water, and varying amounts of snow that interact with 0.5 gkg^{-1} of the accreted cloud species. These calculations suggest that the depositional growth of snow may increase in many cases, while accretion of cloud ice and cloud water could stay the same or be reduced. Reductions in the accretion of cloud ice and water would allow for their retention within the vertical profile, while increases in vapor deposition could explain a slight increase in snow content. However, due to the complex interactions within the iterative forecast model, it is unclear if dynamic processes (subtle changes in updrafts, for example) may also play a role. Increases in cloud water are substantial, however, retention of cloud water within the mixed phase region could be mitigated through other parameterization tunings while still aspiring for an improved representation of snow crystal characteristics.

b. Radar Characteristics

Radar reflectivity is dependent upon the sizes of targets distributed within sampled volumes and the backward scattered component of the active microwave signal. Here, CloudSat reflectivity is simulated by assuming that the true crystal habit is represented by equivalent diameter spheres of uniform density, referred to as "soft spheres" by Liu (2004). The soft sphere formulation tends to overestimate forward scattering in comparison to higher order simulations using a discrete dipole approximation (Liu 2004), therefore, some underestimate of radar reflectivity is expected. Furthermore, Battaglia et al. (2008) have noted that multiple scattering effects allow for a greater 94 GHz reflectivity in areas of moderate to heavy precipitation, despite expectations of significant attenuation. The SDSU utilizes single scattering, therefore, some additional underestimate of CloudSat reflectivity is expected.

CloudSat observations suggest a reflectivity mode around 10 dBZ within the lowest 4 km, followed by a uniform lapse rate to cloud top. Isolated bands of enhanced reflectivity along the flight track produce limited occurrences of reflectivity as high as 15 dBZ (Fig. 7). In the control forecast, the reflectivity mode is generally too low (5 dBZ) and extends too far aloft, reaching to about 6 km. Continuing to cloud top, the reflectivity lapse rate is less than observed. Note that the decrease in the reflectivity mode from 6 km to the surface, not seen in observations, may be due to single scattering and soft sphere assumptions that would combine to reduce radar backscatter. Some improvement in the lower levels is noted in the experimental forecast, where the reflectivity below 4 km is generally increased by a few dB, although structural errors in the height of the low level mode and lapse rate to cloud top remain. Within the experimental forecast, snow crystal characteristics in the lowest levels are expected to include size distributions where the crystals are larger but reduced in number concentration and have densities consistent with the ice-air mixtures of large aggregates (Fig. 6).

At 94 GHz, Mie resonance effects complicate inferences based on reflectivity, as oscillations in radar backscatter develop despite continued increases in the target diameter. The WSR-88D system is a convenient supplement, as the 10-cm wavelength allows for

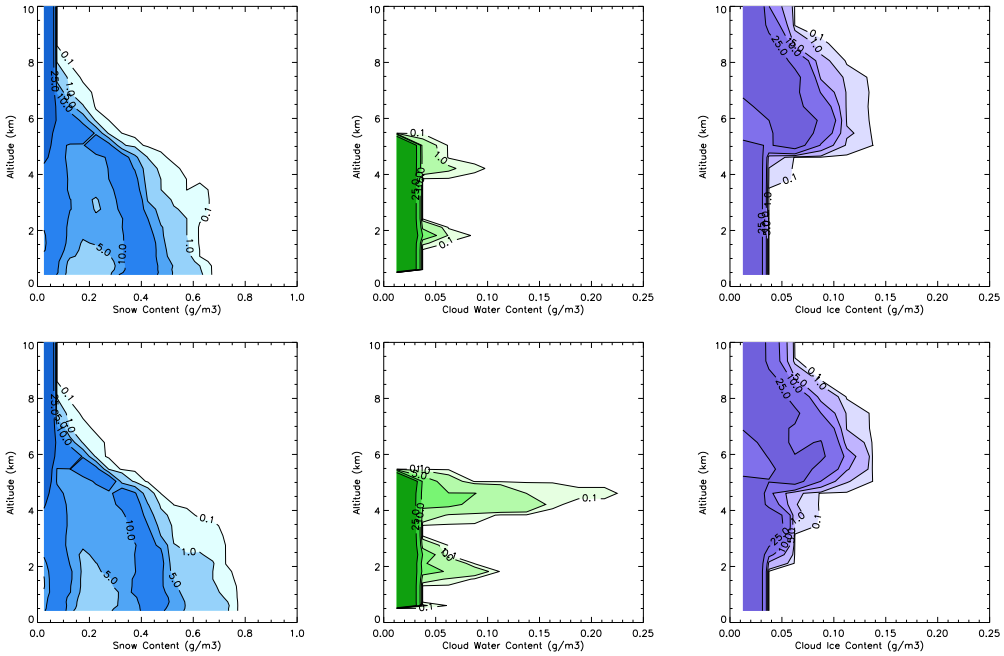

Fig. 5. Contoured frequency with altitude diagrams of model hydrometeor content (gm^{-3}) for the Goddard control case (top) and experimental temperature-based microphysics schemes (bottom), based on profiles extracted from the parallelogram of Fig. 1. Snow, cloud water and cloud ice are displayed from left to right across each row. Note that the bin size magnitudes vary between the snow and nonprecipitating classes.

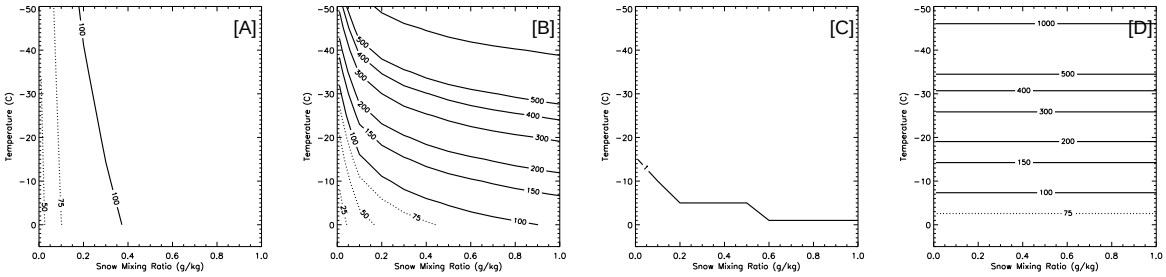

Fig. 6. Percentage change in the magnitude of snow source terms, size distribution characteristics and variations in density due to the inclusion of a temperature-based parameterization, taken as experimental over control. [a] Process of accretion of cloud ice or water byt snow. [b] Vapor deposition to snow crystals. [c] Mask value representing a change to a distribution with larger mean crystal size and decreased number concentration, in the portion of the graphed domain below the labeled contour. [d] Change in snow crystal density.

Rayleigh scattering principles and a steady increase in backscatter that depends upon the sixth moment of the size distribution. In the control forecast, the reflectivity mode present at 94 GHz is apparent once more, with simulated WSR-88D reflectivity of approximately 30 dBZ (Fig. 8). This magnitude of radar return is nearly double the observations, and additionally, simulated reflectivity exhibits a broader range from 20 to 40 dB (varying by level) than the general 20 dB range observed. At a WSR-88D wavelength, the reflectivity lapse rate above 4 km is greater than observed. The incorporation of a temperature based distribution reduces the low level reflectivity mode by approximately 5 dB, although the forecast modal values far exceed observations throughout most of the cloud layer.

When analyses from both systems are considered together, the temperature based distribution seems to improve the reflectivity characteristics at low levels. The control simulation generates too low (high) of a reflectivity at 94 GHz (3 GHz) in the lowest 4 km, with these errors offset partially by the switch to a temperature based distribution. However, errors in the structure of simulated precipitation are evident, notably in the development of a low level mode beyond 4 km. One issue with a temperature based parameterization is the development of isothermal or inversion layers, which then fix the distribution to a uniform value throughout that layer (in the isothermal case, Fig. 9) or awkwardly transition crystal sizes in a manner that is not physically based (in the inversion case). High resolution forecasts

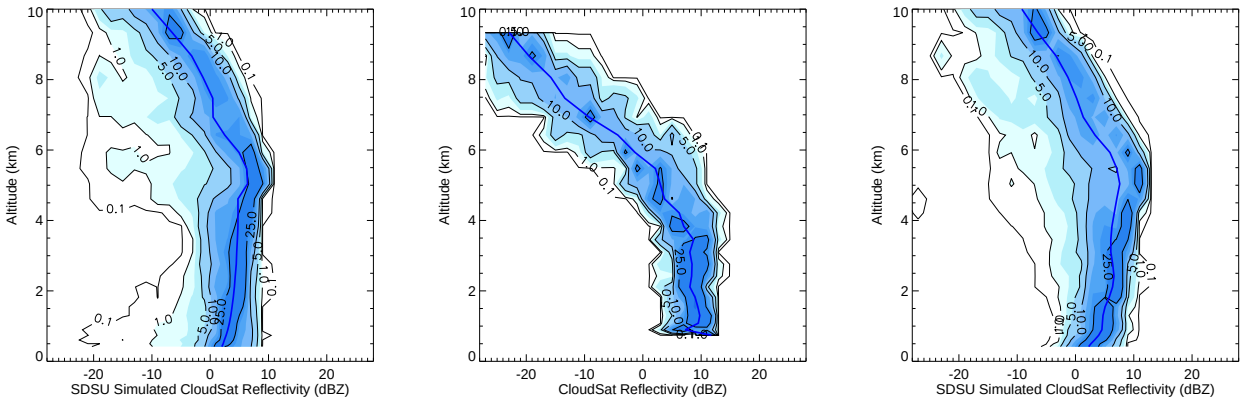

Fig. 7. Contoured frequency with altitude diagrams of CloudSat 94 GHz Cloud Profiling Radar reflectivity, obtained from simulations of model profiles in the original Goddard scheme forecast (left), actual observations of light to moderate snowfall (middle) and model profiles with an experimental temperature dependent density and size distribution (right). Color filled contours are at increments of 1, 2.5, and every 5% thereafter. The median profile is represented as a solid blue line.

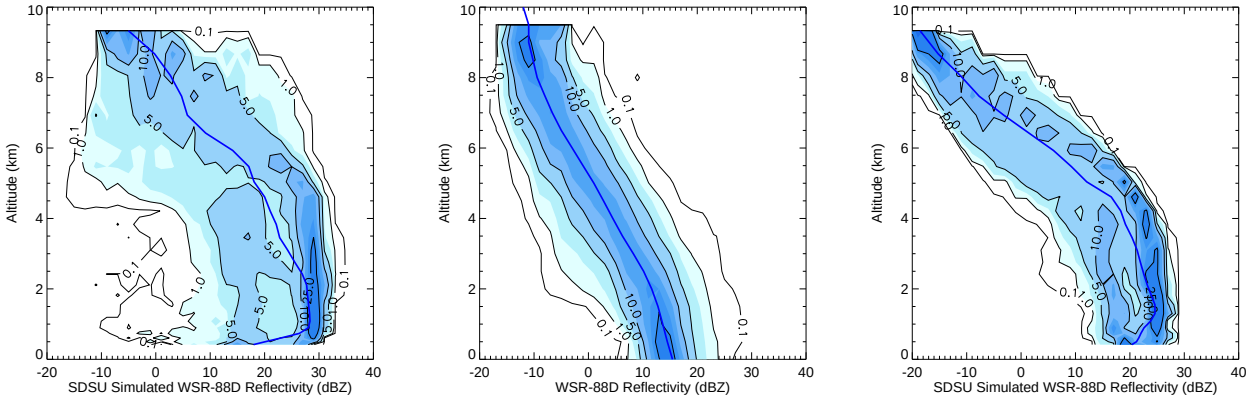

Fig. 8. Contoured frequency with altitude diagrams of WSR-88D, 3 GHz reflectivity, obtained from simulations of model profiles in the original Goddard scheme forecast (left), a half hour of volume scans by the KOAX radar with coverage in the polygon of Fig. 1 (middle) and model profiles with a temperature-dependent density and size distribution (right). Color filled contours are at increments of 1, 2.5, and every 5% thereafter. The median profile is represented as a solid blue line.

simulate the vertical profile of temperature with enough detail that subtle variations from a mean lapse rate may also incorporate artificial and sudden changes in distribution characteristics. Therefore, future work will investigate alternative parameterizations that incorporate temperature or altitude but seek to avoid problems resulting from isothermal or inversion conditions.

4. SUMMARY

Winter storms pose a significant challenge to the operational forecasting community due to uncertainties in precipitation quantity, duration, and type. As high resolution forecast models are increasingly capable of cloud and precipitation permitting simulations rather than coarser parameterizations, verification of cloud structures provide a check for model performance. Two simulations of a winter cyclone were produced using the WRF model: one utilizing the default NASA Goddard single-moment, bulk water microphysics scheme and a second forecast that incorporated snow crystal size distrbution characteristics and bulk density that vary with temperature. Radar remote sensing was utilized to compare observed and simulated precipitation structures, based on reflectivity from the 94 GHz, NASA CloudSat Cloud Profiling Radar and the 3 GHz, WSR-88D located at Omaha, Nebraska.

The inclusion of temperature dependent snow characteristics modifies several parameterized, physical processes that act in various ways to increase the amount of snow, cloud ice, and cloud water throughout the cloud layer, although little change in surface precipitation was noted. The ranges in and extremes of reflectivity values are more appropriately represented in the lowest model levels when temperature dependent characteristics are

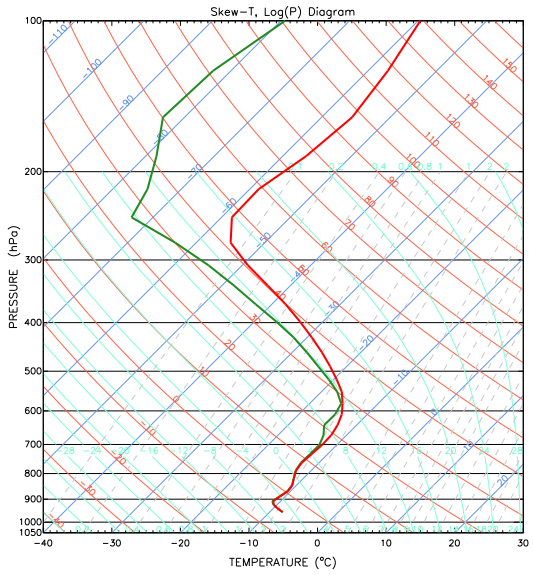

Fig. 9. Mean profile of temperature and dew point among model profiles represented by the polygon of Fig. 1 and used in reflectivity CFAD analyses.

included. Several problems remain, and are related to difficulties in the vicinity of isothermal layers and inversions, where functions of temperature are limited to fixed values and nonphysical transitions to larger or smaller mean crystal sizes. Future work will investigate alternatives, likely based upon a combination of temperature and altitude.

ACKNOWLEDGMENTS

The lead author is supported by the Cooperative Education Program at NASA Marshall Space Flight Center. The authors would like to thank Dr. David Hudak for providing aircraft spiral results from the Canadian CloudSat/CALIPSO Verification Program, as well as Drs. Toshi Matsui, Wei-Kuo Tao and Roger Shi of NASA Goddard Space Flight Center for assistance with the Goddard microphysics scheme and the Satellite Data Simulator Unit.

REFERENCES

Battaglia, A., J. Haynes, T. L'Ecuyer, and C. Simmer, 2008: Identifying multiple-scattering in CloudSat observations over the oceans. *J. Geophys. Res.*, doi:10.1029/2008JD009960.

Bernardet, L., et al., 2008: The development testbed center and its winter forecasting experiment. *Bull. Amer. Met. Soc.*, **89**, 611–627.

Heymsfield, A., A. Bansemer, P. Field, S. Durden, J. Stith, J. Dye, W. Hall, and T. Grainger, 2002: Observations and parameterizations of particle size distributions in deep tropical cirrus and stratiform precipitating clouds: Results from in situ observations in TRMM field campaigns. *J. Atmos. Sci.*, **59**, 3457–3491.

Heymsfield, A., A. Bansemer, C. Schmitt, C. Twohy, and M. Poellot, 2004: Effective ice particle densities derived from aircraft data. *J. Atmos. Sci.*, **61**, 982–1003.

Hudak, D., H. Barker, P. Rodriguez, and D. Donovan, 2006: Winter precipitation studies with a dual polarized C-band radar. *Preprints, European Conference on Radar in Meteorology and Hydrology*, Barcelona, Spain, 18-22 September 2006.

Kain, J., et al., 2008: Severe-weather forecast guidance from the first generation of large domain convection-allowing models: Challenges and opportunities. *Preprints, 24th Conference on Severe Local Storms, Savannah, GA, American Meteorological Society, 12.1*.

Liu, G., 2004: Approxmation of single scattering properties of ice and snow particles for high microwave frequencies. *J. Atmos. Sci.*, **61**, 2441–2456.

Matsui, T., X. Zeng, W.-K. Tao, H. Masunaga, W. Olson, and S. Lang, 2008: Evaluation of long-term cloud resolving model simulations using satellite radiance observations and multi-frequency satellite simulators. *J. Atmos. Ocean. Tech.*, early online release.

Miller, M., J. Verlinde, C. Gilbert, G. Lehenbauer, J. Tongue, and E. Clothiaux, 1998: Detection of nonprecipitating clouds with the WSR-88D: A theoretical and experimental survey of capabilities and limitations. *Weather and Forecasting*, **13**, 1046–1062.

Ryan, B., 2000: A bulk parameterization of the ice particle size distribution and the optical properties in ice clouds. *J. Atmos. Sci.*, **57**, 1436–1451.

Stephens, G., et al., 2002: The CloudSat mission and the A-Train. *Bull. Amer. Meteor. Soc.*, **83**, 1771–1790.

Tao, W.-K., J. Shi, S. Chen, S.-Y. Hong, C. Peters-Lidard, S. Braun, and J. Simpson, submitted: Revised bulk-microphysical schemes for studying precipitation processes. Part I: Comparisons with other schemes. *Mon. Wea. Rev.*

Yuter, S. and R. Houze, 1995: Three-dimensional kinematic and microphysical evolution of florida cumulonimbus. Part II: Frequency distributions of vertical velocity, reflectivity and differential reflectivity. *Mon. Wea. Rev.*, **123**, 1941–1963.